AIAA JOURNAL
Vol. 35, No. 2, February 1997

Comparative Study of Inflow Conditions for Spatially Evolving Simulation

Yong Mann Chung* and Hyung Jin Sung†
Korea Advanced Institute of Science and Technology, Yusong-ku, Taejon 305-701, Republic of Korea

A new spatiotemporal inflow condition is devised and evaluated with other methods, i.e., temporal, phase jittering and amplitude jittering, and random noise. These methods are validated by testing a large-eddy simulation of turbulent channel flow. Computational results are presented to disclose the ability of inflow conditions to capture the turbulent statistics with correct phase information and dynamics. The present spatiotemporal inflow condition is found to be generally satisfactory in CPU time and data management.

Introduction

MOST direct numerical simulations and large-eddy simulations (LES) have been restricted to simple flows because of the limitation of available computer resources. In particular, periodic boundary conditions were generally employed to avoid the difficulties associated with the inflow and outflow conditions. However, it has been learned that a substantial difference in the growth rate of unstable waves exists between spatial and temporal simulations, although the results agree in a global sense.[1] For a direct comparison with experimental results, it is highly desirable to perform spatial simulations rather than temporal simulations with periodic boundary conditions.

To simulate spatially evolving flows correctly, implementation of a robust inflow condition, with a suitable outflow condition, is of prime importance. The proper outflow condition makes the flow pass through the exit boundary with little distortion, so that the interior solution is not polluted by errors from the exit boundary. A literature survey reveals that there have been many attempts to deal with the outflow conditions in spatially evolving flows. Among others, Pauley et al.[2] developed the convective boundary condition for an unsteady separated boundary layer, which was modified later by Wang et al.[3] for an acoustic problem. Several buffer domain techniques, in which the governing equations were changed to the parabolic type, also have been developed.[4] Nonreflecting boundary conditions are compiled in the review article of Givoli.[5]

Implementation of an appropriate inflow condition is more difficult to deal with than the outflow condition, because the influence of the inflow condition persists over large distances downstream.[6] A perusal of the literature indicates that studies on the implementation of inflow condition are relatively scarce. Turbulent kinetic energy should be continuously supplied by the inflow condition to maintain turbulence. In this sense, a simple time-mean velocity is not adequate as an inflow condition, because it can make the flow become laminar. To overcome this drawback, a random noise of small amplitude was superimposed on the time-mean velocity to model the residual turbulence within the upstream flow.[7] Although turbulent kinetic energy could be supplied with the random noise, the dependence of the turbulent kinetic energy on inhomogeneous directions was not taken into account, nor was the correct phase information between each velocity component. To impose a real turbulence at the inflow boundary, instantaneous flow data from an auxiliary inflow simulation of a fully developed turbulent channel/boundary layer flow should be supplied with the same Reynolds number and grid spacings. Hereafter, this method is designated as temporal. The main advantage of this inflow condition is that it can provide a turbulent inflow with correct phase information and dynamics. However, this temporal method calls for additional CPU time and large data management and storage capacity.

Temporal inflow data can be replaced by spatial inflow data by using Taylor's frozen-field hypothesis. On the basis of this hypothesis, spatial inflow data can be extracted by sweeping upstream with an appropriate constant velocity. To apply this procedure, however, an extremely long spatial field is needed to supply inflow data continuously during the entire computational run. If a finite length of channel is adopted, the inflow spatial data should be used repeatedly. To destroy the periodicity caused by the repeated usage of an inflow field, it is necessary to modify the original inflow data to some extent for every cycle. In Fourier transform space, we can change the amplitude and phase of the energy spectrum of the inflow data by means of random numbers for every cycle, to supply fresh data. These methods are referred to as amplitude jittering[8] and phase jittering,[9,10] respectively. It is found that amplitude jittering can contain correct flow structures whereas phase jittering can reproduce the exact energy spectrum of the real turbulent flow. For phase jittering, however, it is well known that an adjustment zone of a considerable length is necessary to allow for the flow to evolve into real turbulence,[11] whereas some improvement is achieved by amplitude jittering.[8]

In the present study, flowfields of a temporal simulation at several time instants are adopted as an inflow condition, instead of the repeated usage of one flowfield at a time step. The present spatiotemporal method encompasses the advantage of instantaneous inflow data as well as that of spatial inflow data with Taylor's hypothesis. By combining these merits, a promising method is devised. The main objective is to evaluate these several inflow conditions and to provide a simple, but physically plausible inflow condition, which is highly desirable for a successful simulation of spatially evolving flows. These methods are validated by testing a LES of turbulent channel flow.

Inflow Conditions

Temporal: Instantaneous Velocity Field

In the simulation of spatially evolving flow, random numbers or sinusoidal fluctuations are simply superimposed to supply turbulent kinetic energy for the flowfield. For example, a random noise of small amplitude was superimposed to model the residual turbulence in the backward-facing step LES of Silveira et al.[7] The random noise cannot produce physically correct behavior of the flow near the wall, for instance, the streaky structures. Hereafter, this method is referred to as random noise.

At the inflow boundary, it is natural to use instantaneous data from an auxiliary inflow simulation of a fully developed turbulent channel flow[12] or a boundary layer.[13] The auxiliary inflow simulation should be performed, with periodic boundary conditions, at the same Reynolds number, with identical grid spacings, to the main spatially evolving simulation. Otherwise, inflow data should be filtered onto a main mesh. As sketched in Fig. 1, the instantaneous

Received Jan. 24, 1996; revision received Oct. 17, 1996; accepted for publication Oct. 24, 1996; also published in *AIAA Journal on Disc*, Volume 2, Number 2.

*Graduate Student, Department of Mechanical Engineering, 373-1 Kusong-dong.
†Professor, Department of Mechanical Engineering, 373-1 Kusong-dong. Member AIAA.

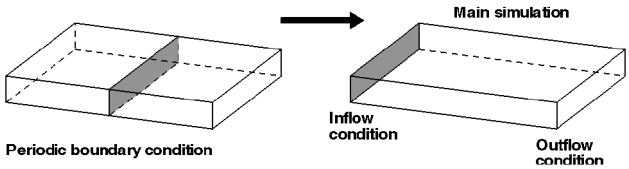

Fig. 1 Schematic diagram for temporal method.

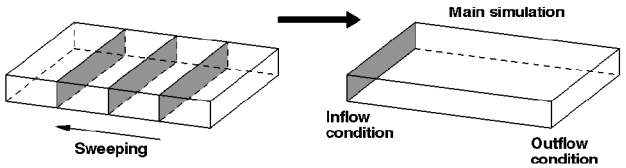

Fig. 2 Schematic diagram for spatial method.

velocity field on a plane perpendicular to the streamwise direction should be stored at each time step. The data are then used at the inlet plane to specify the inflow condition:

$$u_i(0, y, z, t) = v_i(x_c, y, z, t) \tag{1}$$

where $u_i(0, y, z, t)$ represents the velocity of the main simulation at the position $(x = 0, y, z)$ and $v_i(x_c, y, z, t)$ is the velocity of the auxiliary inflow simulation in the y–z plane at time t and $x = x_c$.

It is known that the inflow data taken from an auxiliary inflow simulation can supply an ideal inflow condition in the spatially evolving simulation.[12,13] This is based on the fact that not only the correct near-wall behavior of each Reynolds stress component from a statistical point of view can be described, but also the dynamic characteristics of flow structure, such as the wall streaks in an unsteady viewpoint, may be portrayed. As mentioned earlier, however, this method requires additional CPU time, data management, and storage capacity. This has discouraged researchers from adopting this as an inflow boundary condition.

Spatial: Taylor's Hypothesis

As an alternative to the aforestated temporal method, spatial data can be applied as an inflow condition by utilizing Taylor's frozen-field hypothesis. The roles of space and time are exchanged by assuming that the whole flow structures pass as a frozen field:

$$u_i(0, y, z, t) = v_i(L - U_c t, y, z, t_c) \tag{2}$$

where U_c represents the convection velocity and t_c denotes a certain time instant. Here, L is the streamwise length of the spatial data at t_c. The applicability of Taylor's hypothesis with a constant convection velocity is a central assumption in this approach.[9]

Because an inflow field is provided continuously with a time period equivalent to the channel length L divided by the convection velocity U_c, the inflow channel/boundary-layer data would have to be very long to provide inflow data during the computation time. However, such an extremely long inflow channel is impractical. As an alternative, it is useful to select a moderate length L of inflow channel repeatedly:

$$u_i(0, y, z, t) = v_i(L - x\prime, y, z, t_p) \tag{3}$$

In Eq. (3), t for u_i is related to $x\prime/U_c$ for v_i, where $0 \leq x\prime \leq L$, $x = x\prime + nL$, n is an integer for the repeated usage. As shown in Fig. 2, the inflow condition is provided by sweeping the channel for a time period of L/U_c. However, the periodicity due to the repeated usage of the inflow field poses serious problems. This is because the repeated periodic flow is not a real turbulent flow but a turbulent-like flow. To destroy the periodicity, it is necessary to modify the original inflow data to some extent for every cycle. The complex Fourier coefficients $\hat{u}$ of velocity fluctuations $u\prime$ can be defined as

$$\hat{u}(y, k_z, \omega, t) = \sqrt{E_{uu}(y, k_z, \omega)}\, \exp[i\phi(y, k_z, \omega)t] \tag{4}$$

where $E_{uu}(y, k_z, \omega)$ is the energy spectrum of $u\prime$ at y, $\phi(y, k_z, \omega)$ the phase angle and $i = \sqrt{-1}$. Here, y denotes the wall-normal coordinate, k_z the spanwise wave number, and ω the frequency.

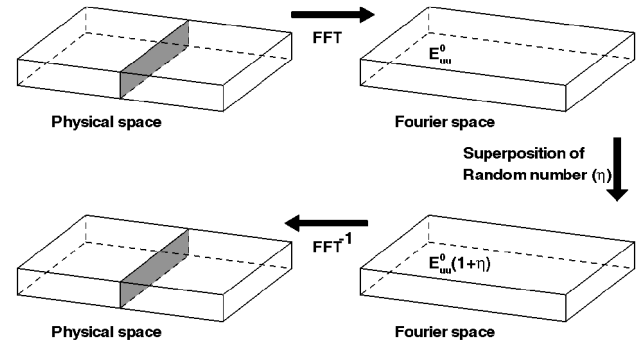

Fig. 3 Schematic diagram for amplitude jittering.

Because the Fourier coefficients of a flow variable are prescribed in terms of phase and amplitude (or magnitude), it is natural to modify each part to obtain new data fields that are different from cycle to cycle.

Phase Jittering

A method was developed by Lee et al.[9] that generates turbulent inflow data with known energy spectrum. For decaying isotropic turbulence, a one-dimensional normalized energy spectrum was used as a target spectrum. The phase angle of the Fourier coefficients at y is a function of frequency ω and transverse wave numbers k_z, i.e., $\phi(y, k_z, \omega)$. In phase jittering, the Fourier coefficient can be changed using a random phase angle at each frequency ω and wave number k_z so as to destroy the periodicity in time:

$$\phi^n(y, k_z, \omega) = \phi^{n-1}(y, k_z, \omega) + \eta(y, k_z, \omega) \tag{5}$$

where $\phi^n(y, k_z, \omega)$ denotes the phase angle for the nth time interval and $\eta(y, k_z, \omega)$ represents a random number. Because the random phase angles have functional dependence on time, the phase randomness determines the smoothness of the generated data. The weak dependence of the phase generates data close to the target spectrum, but a rather periodic temporal signal is produced. The reproduction of almost the exact energy spectrum is an essential part of this method.

Amplitude Jittering

Without changing the phase, random numbers of a certain level are superimposed on the amplitude of the original energy spectrum[8]:

$$E_{uu}(y, k_z, \omega) = E^0_{uu}(y, k_z, \omega)(1 + \eta) \tag{6}$$

where $E^0_{uu}(y, k_z, \omega)$ denotes the original energy spectrum of $u\prime$ at y and η is a random number of fixed magnitude. As displayed in Fig. 3, random numbers with magnitude of roughly 10–20% of the amplitude of the Fourier coefficients are usually superimposed on the original spectrum, and then the inverse Fourier transform is performed. If the magnitude of the random numbers is very small, the original periodicity is recovered, i.e., the generated temporal data are periodic in time. Because the phase information is not changed, it was shown that the flow structures are maintained even with different values of $\eta(\eta \leq 0.2)$.[8] For wall-bounded turbulent flows, amplitude jittering seems to be superior to phase jittering, because flow structures are not destroyed by the former.

Spatiotemporal: Present Method

Amplitude jittering can sustain correct flow structure, whereas phase jittering can produce the exact energy spectrum of real turbulent flow. As stated earlier, an adjustment zone of a considerable length is necessary in the phase jittering method to allow for the flow to evolve into real turbulence.[11] The necessity of the adjustment zone is the main disadvantage of the jittering method, although it is less severe for amplitude jittering.

To be a physically correct inflow condition, both dynamics and phase information of the flow should be maintained. Among the preceding inflow conditions, the temporal method maintains these features. However, because the implementation of the inflow condition is very expensive, a simple inflow condition is proposed.

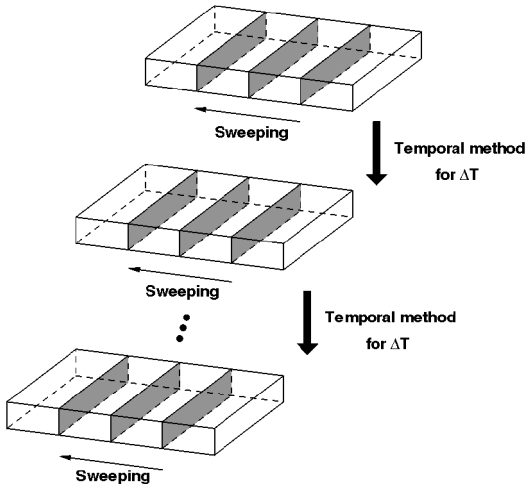

Fig. 4 Schematic diagram for spatiotemporal method.

Flowfields of a temporal simulation at several time instants are used, instead of the repeated usage of one flowfield at a certain time step. The present method utilizes the advantages of the temporal method and the spatial method of Taylor's hypothesis. As described in Fig. 4, each flowfield can provide inflow data for a time period of L/U_c by sweeping the channel with U_c. During the interval (ΔT) from one inflow field to the next, the instantaneous data are then used as an inflow condition, i.e., the temporal method is adopted:

$$u_i(0, y, z, t) = v_i(L - x/U_c, y, z, t_p), \qquad T_0 - L/U_c \leq t \leq T_0 \tag{7}$$

$$u_i(0, y, z, t) = v_i(0, y, z, t), \qquad T_0 \leq t \leq T_0 + \Delta T \tag{8}$$

Because several velocity fields at several time instants are used in the present method, the selection of temporal separation (ΔT) is a central issue that is strongly related to the quality of the inflow condition. If ΔT is very small, inflow velocity fields then will be almost the same as each other. For the other limiting case, a very large temporal separation makes this inflow condition return to the instantaneous data from an auxiliary simulation, which we tried to avoid. This numerical parameter must be selected carefully. Because turbulent flows are correlated in time, independent observations can be made only at intervals larger than the time scale h/u_τ of the large-scale turbulent motion. Here, h denotes the half channel height and u_τ is the friction velocity. It is desirable to use the inflow data for the time period of h/u_τ to secure statistically independent inflow data. Several independent velocity fields with the temporal separation of h/U_m are tested to cover the inflow fields with the time period of $h/u_\tau(\Delta T = 1)$.

Numerical Method

The governing equations are derived by applying the filtering operation to the incompressible Navier–Stokes and continuity equations. Filtering is accomplished by integrating the equations over a control volume. Finally, we obtain the dynamic equations of the large-scale flowfield:

$$\frac{\partial \bar{u}_i}{\partial t} + \frac{\partial}{\partial x_j}(\bar{u}_i \bar{u}_j) = -\frac{\partial \bar{p}}{\partial x_i} - \frac{\partial}{\partial x_j}\tau_{ij} + \frac{1}{Re}\frac{\partial^2 \bar{u}_i}{\partial x_j \partial x_j} \tag{9a}$$

$$\frac{\partial \bar{u}_i}{\partial x_i} = 0 \tag{9b}$$

where the overbar denotes the filtering operation. In these equations, u_i are the velocity components, τ_{ij} the residual stress tensor, and Re the Reynolds number.

All terms in these equations are resolved in the LES except the residual stress tensor

$$\tau_{ij} = \overline{u_i u_j} - \bar{u}_i \bar{u}_j \tag{10}$$

which must be modeled. Based on the most commonly used Smagorinsky model,[14] the eddy viscosity model is obtained by assuming that the small scales are in equilibrium, so that energy production and dissipation are in balance. This yields an expression of the form

$$\tau_{ij} - 1/3\delta_{ij}\tau_{kk} = -2\nu_t \bar{S}_{ij} \tag{11}$$

$$\nu_t = (C_S \Delta)^2 |\bar{S}| \tag{12}$$

where C_S is the constant to be determined and Δ is the filter width, $|\bar{S}| = \sqrt{(2\bar{S}_{ij}\bar{S}_{ij})}$. The large-scale strain-rate tensor is represented as

$$\bar{S}_{ij} = \frac{1}{2}\left(\frac{\partial \bar{u}_i}{\partial x_j} + \frac{\partial \bar{u}_j}{\partial x_i}\right) \tag{13}$$

In the present simulations, we used a dynamic subgrid-scale model developed by Germano et al.[15] In this model, the constant C_S is computed dynamically as the calculation progresses.

A fractional-step method for solving the filtered Navier–Stokes equations is employed[16,17] that is based on a time-splitting method in conjunction with the approximate factorization technique. The solution procedure consists of semi-implicit approach using the third-order Runge–Kutta method for the nonlinear convective terms and the implicit Crank–Nicolson method for the viscous terms. For spatial discretization, second-order central differences were used on a staggered grid.

Numerical stability is limited by an explicit treatment of the convective terms. The stability limit, defined as $\max(|u_i/\Delta_i|)\Delta t$, is $\sqrt{3}$, based on the total time step Δt. The accuracy of the fractional-step method is second order in time. The Poisson equation for the pressure correction in the fractional-step method is solved in wave-number space by transformation of variables into one-dimensional discrete Fourier series.

Results and Discussion

First, it is important to ascertain the reliability and accuracy of the present large-eddy simulation. This forms an integral part of the overall validation efforts. An assessment of the present simulations are made by comparing the numerical results to well-confirmed data.

A fully developed turbulent channel flow with periodic boundary conditions is simulated. The Reynolds number of the channel based on the mean velocity U_m and the half channel height h is $Re_h = 2.8 \times 10^3$. This corresponds to $Re_\tau = 1.8 \times 10^2$, based on the friction velocity u_τ. The streamwise and spanwise dimensions of the computational domain are set to be $12h$ and $4h$, respectively. These values are much larger than the critical values needed to sustain the turbulence in the flow.[18] With a grid system ($64 \times 64 \times 64$ in the x, y, z directions, respectively), the streamwise and spanwise grid resolutions are $\Delta x^+ = 34$ and $\Delta z^+ = 11.2$, respectively. The grid stretching was implemented along the wall-normal direction to resolve the near-wall structures.

The present results are compared with the LES of Cabot,[19] which also is obtained by LES with periodic boundary conditions. The main differences between the present LES and Cabot's (LES) results are the numerical scheme and different model of backscattering. Even though these details are different, as shown in Fig. 5, the turbulence quantities of the present simulation are in close agreement with the results of Cabot. This exemplifies the reliability of the present simulation.

Now, the performance of several inflow conditions in a turbulent channel flow is examined. Three inflow conditions are selected, with the convective boundary condition at the exit.[2] For comparison, the result with periodic boundary conditions also is represented. For all cases calculated in the present study, the computed results exhibit consistent convergence characteristics. The notation periodic represents the result with periodic boundary conditions imposed. As shown in Fig. 6, the time-mean turbulent qualities are not much affected by the inflow conditions. These trends are the same in the profiles of the time-mean velocity (not presented here). The overall agreement of the three inflow conditions is satisfactory.

To see the ability of inflow conditions to capture the turbulent structures, the instantaneous streamwise velocity profiles in an $x-y$ plane are shown in Fig. 7, together with contours of the streamwise velocity fluctuation in the $x-z$ plane at $y^+ = 10$. All velocities are

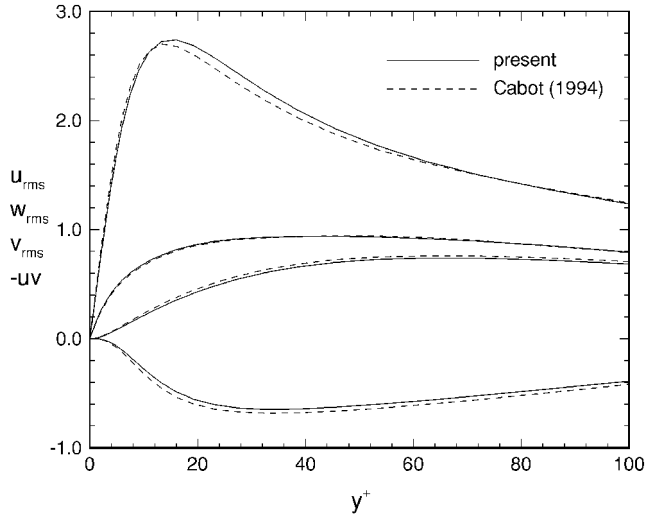

Fig. 5 Comparison of Reynolds stresses with Cabot results[19] ($Re_\tau = 1.8 \times 10^2$).

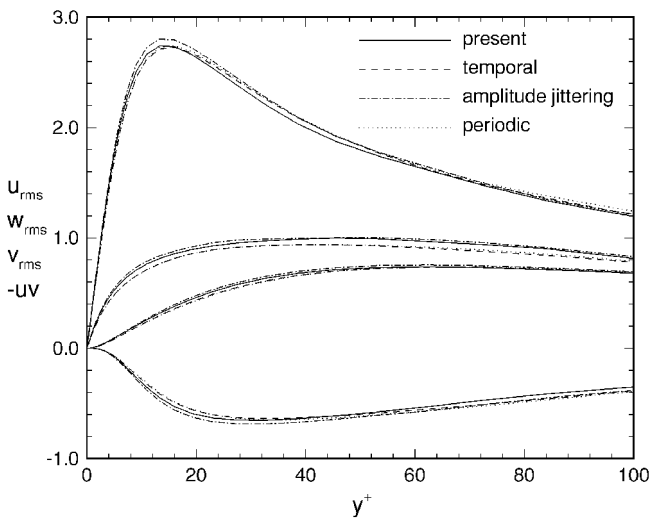

Fig. 6 Comparison of Reynolds stresses with three inflow conditions ($Re_\tau = 1.8 \times 10^2$).

normalized by the freestream mean velocity U_m. The negative contours are plotted with dotted lines and the positive contours with solid lines. Among the most important structures in the near-wall region are the low-speed streaks. The mean streak spacing in wall units, which was calculated from the two-point correlations, is about 100. Low-speed streaks are clearly discernible when the present method (Fig. 7a) and the temporal method (Fig. 7b) are employed. When the amplitude jittering ($\eta = 0.2$) is applied (it is seen in Fig. 7c), the structure is slightly destroyed. To clarify the distinction, the correlation $R_{uu}(\Delta z) = \langle u(x, y, z, t)u(x, y, z + \Delta z, t)\rangle$ at $y^+ = 10$ is displayed for $x = 1$ and $x = 6$ (Fig. 8), respectively. The correlation by the amplitude jittering is shown to be slightly deviated at $x = 1$; however, it recovers soon ($x = 6$). As mentioned earlier, the near-wall structures can be maintained, depending on the amplitude of random numbers used in the amplitude jittering. When the amplitude is small, the flow structure is sustained, but with increased periodicity. If larger-amplitude random numbers are adopted, the quality of inflow degenerates considerably. Finally, it is clear that the structure is not sustained at all when random noise is employed (Fig. 7d).

Comparisons are extended to the profiles of the skin-friction coefficient C_f in the streamwise direction (Fig. 9). If inflow data have some physically meaningful flow structures, the inflow data can adjust to the real turbulence within a few grid spacings. This is because the flow loses its statistical characteristics within the first few grid points. However, it was found in Fig. 7 that superimposed

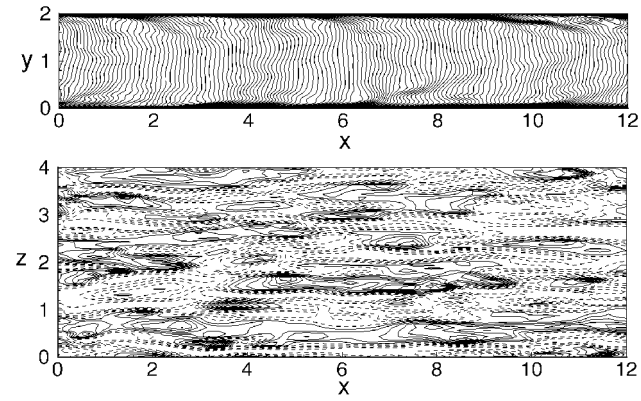

a) Present

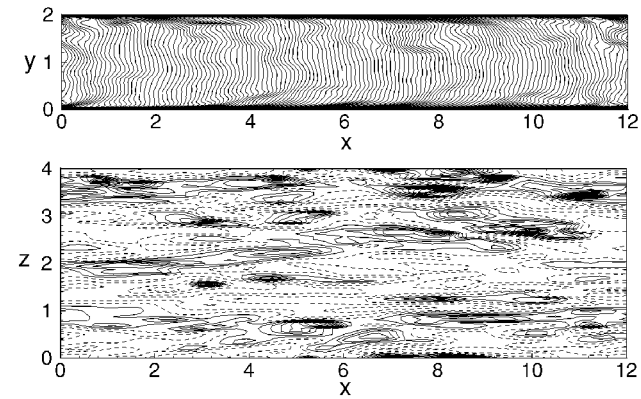

b) Temporal

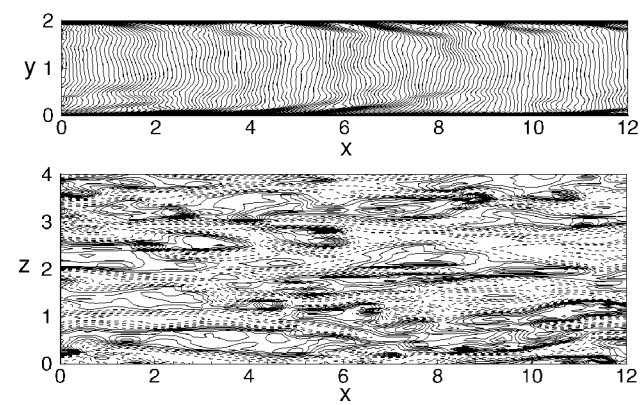

c) Amplitude jittering

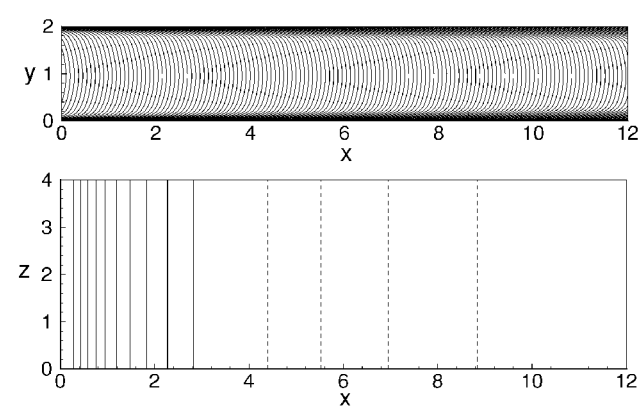

d) Random noise

Fig. 7 Instantaneous streamwise velocity profiles in an x–y plane and contours of the streamwise velocity fluctuation in an x–z plane at $y^+ = 10$.

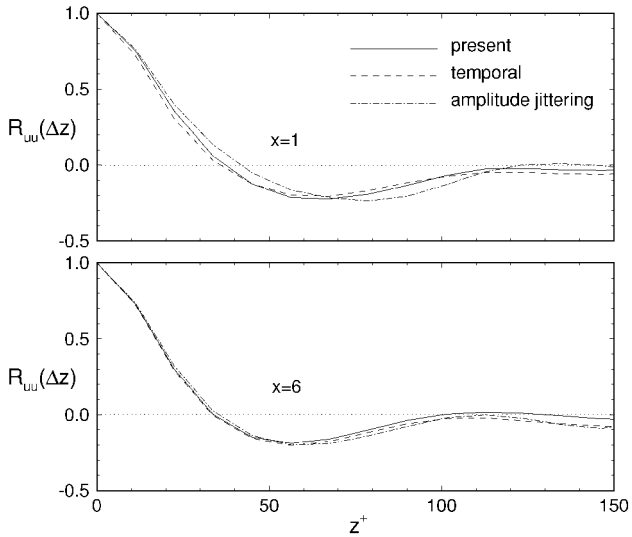

Fig. 8 Profiles of $R_{uu}(\Delta z) = \langle u(x, y, z, t)\, u(x, y, z + \Delta z, t) \rangle$ at $y^+ = 10$ for $x = 1$ and $x = 6$.

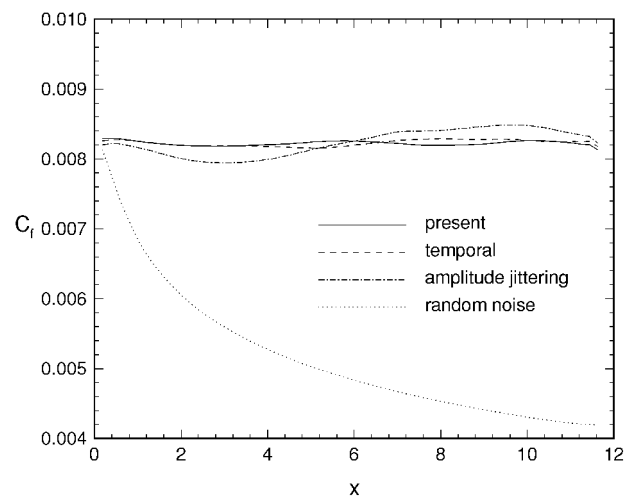

Fig. 9 Profiles of C_f for $Re_\tau = 1.8 \times 10^2$ with several inflow conditions.

random noise cannot maintain turbulent flow structure. This means that superimposed random noise is not adequate as a turbulent inflow condition for spatially evolving simulation. In spite of the exact reproduction of the turbulent statistics, a so-called adjustment zone, with a considerable length, is necessary to allow for the inflow to evolve to real turbulence. As shown in Fig. 9, for random noise, the friction coefficient loses approximately 25% of its channel value, from the initial value of 8×10^{-3}, within $x = 2$. This initial transition and apparent laminarization is due to the unphysical inflow turbulence, which is a result of the random noise. For phase jittering, it was reported that, in the flow over a backward step, an adjustment zone longer than 10 times the step height is needed to ensure the recovery of the turbulent boundary layer.[11] The necessity of the long adjustment zone is one of the main disadvantages in phase jittering.

Contrary to the random noise method, the present method gives a reasonable C_f prediction, comparable with the temporal method. This result is expected because the flow structure is fully sustained (Fig. 7). A small adjustment zone ($0 < x < 5$) can be found in the C_f profile when the amplitude jittering is employed ($\eta = 0.2$). As stated earlier, the size of the adjustment zone is directly connected with the amplitude of the random number (η). If a large-amplitude random number is adopted, the quality of the inflow degenerates considerably, despite the diminished periodicity.

The capabilities of the present method are examined by comparing its CPU and computer memories against the other methods. Toward this end, comparisons of the present method with those of the other inflow methods are summarized in Table 1. The computations were performed on a Cray YMP-C90. Clearly, as anticipated, the present method performs better than the temporal method in both CPU time and data memory. It is seen that the CPU time and memory requirements for three of the methods are comparable, i.e., spatiotemporal, amplitude jittering, and random noise.

Table 1 Comparison of CPU time and computer memory among five inflow conditions with a $64 \times 64 \times 64$ grid system

Inflow condition	CPU time, h	Memory, MW
Present	5.18	8.41
Temporal	8.29	15.23
Amplitude jittering	5.13	8.41
Random noise	4.55	7.53

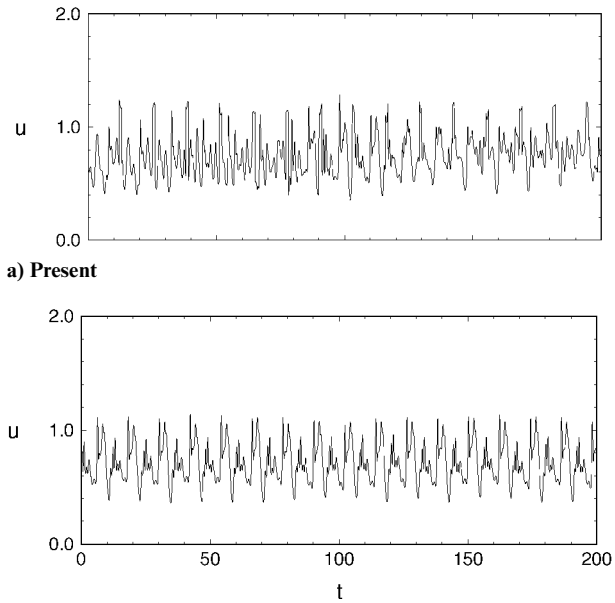

a) Present

b) Amplitude jittering

Fig. 10 Instantaneous streamwise velocity fluctuations at $y^+ = 10$.

Finally, the instantaneous u-component velocity fluctuations at $y^+ = 10$ are displayed in Fig. 10. Two methods, i.e., the present method and the amplitude jittering, are selected to check the periodicity. Amplitude jittering seems to be recommendable as an inflow condition. However, periodicity is clearly discernible.

Concluding Remarks

To simulate spatially evolving flows, a new spatiotemporal inflow condition was devised and evaluated. The present spatiotemporal method was compared with other methods, i.e., temporal, amplitude jittering, and random noise. These evaluations were made by testing a large-eddy simulation of turbulent channel flow. It was found that the time-mean velocity and turbulence intensities are not much affected by the inflow conditions. The temporal method provides the turbulent inflow with correct phase information and dynamics. However, additional CPU time and memory are needed. Although phase jittering generates the exact turbulence statistics, it cannot sustain the flow structure in wall-bounded flows. If phase jittering is imposed for a wall-bounded flow, an adjustment zone of considerable length is necessary to allow for the inflow to evolve to real turbulence. Amplitude jittering can maintain the near-wall structures. However, the periodicity is discernible and the results depend on the amplitude of random numbers used to destroy the periodicity.

References

[1] Saiki, E. M., Biringen, S., Danabasoglu, D., and Street, C. L., "Spatial Simulation of Secondary Instability in Plane Channel: Comparison of K- and H-Type Disturbances," *Journal of Fluid Mechanics*, Vol. 253, 1993, pp. 485–507.

[2]Pauley, L. R., Moin, P., and Reynolds, W. C., "The Structure of Two-Dimensional Separation," *Journal of Fluid Mechanics*, Vol. 220, 1990, pp. 397–411.

[3]Wang, M., Lele, S. K., and Moin, P., "Sound Radiation During Local Laminar Breakdown in a Low-Mach-Number Boundary Layer," *Journal of Fluid Mechanics*, Vol. 319, 1996, pp. 197–218.

[4]Colonius, T., Lele, S. K., and Moin, P., "Boundary Conditions for Direct Computation of Aerodynamic Sound Generation," *AIAA Journal*, Vol. 31, No. 9, 1993, pp. 1574–1582.

[5]Givoli, D., "Non-Reflecting Boundary Conditions," *Journal of Computational Physics*, Vol. 94, 1991, pp. 1–29.

[6]Rogallo, R. S., and Moin, P., "Numerical Simulation of Turbulent Flows," *Annual Review of Fluid Mechanics*, Vol. 16, 1984, pp. 99–137.

[7]Silveira Neto, A., Grand, D., Métais, O., and Lesieur, M., "A Numerical Investigation of the Coherent Vortices in Turbulence Behind a Backward-Facing Step," *Journal of Fluid Mechanics*, Vol. 256, 1993, pp. 1–25.

[8]Na, Y., "Direct Numerical Simulation of Turbulent Boundary Layers with Adverse Pressure Gradient and Separation," Ph.D. Thesis, Dept. of Mechanical Engineering, Stanford Univ., Stanford, CA, 1996.

[9]Lee, S., Lele, S., Ferziger, J., and Moin, P., "Simulation of Spatially Evolving Turbulence and the Applicability of Taylor's Hypothesis in Compressible Flow," *Physics of Fluids*, Vol. A4, No. 7, 1992, pp. 1521–1530.

[10]Handler, R. A., Levich, E., and Sirovich, L., "Drag Reduction in Turbulent Channel Flow by Phase Randomization," *Physics of Fluids*, Vol. A5, No. 3, 1993, pp. 686–694.

[11]Le, H., and Moin, P., "Direct Numerical Simulation of Turbulent Flow over a Backward-Facing Step," Dept. of Mechanical Engineering, Stanford Univ., Rept. TF-58, Stanford, CA, Dec. 1995.

[12]Arnal M., and Friedrich, R., "Large-Eddy Simulation of a Turbulent Flow with Separation," *Turbulent Shear Flows 8*, edited by F. Durst, R. Friedrich, B. E. Launder, F. W. Schmidt, U. Schumann, and J. H. Whitelaw, Springer–Verlag, Berlin, 1993, pp. 169–187.

[13]Voke, P., and Yang, Z., "Numerical Study of Bypass Transition," *Physics of Fluids*, Vol. 7, No. 9, 1995, pp. 2256–2264.

[14]Smagorinsky, J., "General Circulation Experiments with the Primitive Equations. I. The Basic Experiment," *Monthly Weather Review*, Vol. 91, No. 3, 1963, pp. 99–164.

[15]Germano, M., Piomelli, U., Moin, P., and Cabot. W. H., "A Dynamic Subgrid-Scale Eddy Viscosity Model," *Physics of Fluids*, Vol. 3, No. 7, 1991, pp. 1760–1765.

[16]Kim, J., and Moin, P., "Application of a Fractional-Step Method to Incompressible Navier–Stokes Equations," *Journal of Computational Physics*, Vol. 59, 1985, pp. 308–323.

[17]Le., H., and Moin, P., "An Improvement of Fractional Step Methods for the Incompressible Navier–Stokes Equations," *Journal of Computational Physics*, Vol. 92, 1991, pp. 369–379.

[18]Jimenez, J., and Moin, P., "The Minimal Flow Unit in Near-Wall Turbulence," *Journal of Fluid Mechanics*, Vol. 225, 1991, pp. 213–240.

[19]Cabot, W., "Local Dynamic Subgrid-Scale Models in Channel Flow," *Annual Research Briefs 1994*, Center for Turbulence Research, Dept. of Mechanical Engineering, Stanford Univ., Stanford, CA, 1994, pp. 143–159.